Chemical Engineering Journal 426 (2021) 130856

Contents lists available at ScienceDirect

Chemical Engineering Journal

journal homepage: www.elsevier.com/locate/cej

Biocatalytic micromixer coated with enzyme-MOF thin film for CO_2 conversion to formic acid

Milton Chai [a,1], Sajad Razavi Bazaz [b,1], Rahman Daiyan [c], Amir Razmjou [d,a,*], Majid Ebrahimi Warkiani [b], Rose Amal [c], Vicki Chen [e,a]

[a] UNESCO Centre for Membrane Science and Technology, School of Chemical Engineering, The University of New South Wales, Sydney, NSW 2052, Australia
[b] School of Biomedical Engineering, University of Technology Sydney, Sydney, NSW 2007, Australia
[c] Particles and Catalysis Research Laboratory, School of Chemical Engineering, The University of New South Wales, Sydney, NSW 2052, Australia
[d] Centre for Technology in Water and Wastewater, University of Technology Sydney, Ultimo, New South Wales 2007, Australia
[e] School of Chemical Engineering, University of Queensland, St. Lucia, Queensland 4072, Australia

ARTICLE INFO

Keywords:
Micromixer
Biocatalysis
Metal-organic framework
Thin film
Fuel cell

ABSTRACT

In this study, a novel micromixer with a 3D helical, threaded channel was fabricated via 3D printing. The micromixer can enhance the mass transfer of reactants and product in an enzymatic cascade reaction converting CO_2 to formic acid. Two enzymes, including carbonic anhydrase (CA) and formate dehydrogenase (FDH), were biomineralised in a zeolitic imidazolate framework-8 composite thin film on the micromixer channel that has been modified with polydopamine/polyethyleneimine. The biocatalytic performance of the micromixer was evaluated by testing at various liquid flow rates, and an optimum liquid flow rate at 1 mL/min ($Re_l = 8$, $De_l = 3$) was observed as the two-phase flow pattern in the micromixer channel transitioned from slug flow to bubbly flow. A comparison of the micromixer performance with and without threaded channels revealed ~ 170% enhancement in formic acid yield, indicating improved mixing with the presence of threads. In addition, the formic acid production rate for the micromixer with threaded channel was three folds higher than a conventional bubble column, demonstrating the superior performance of the proposed micromixer. The ease of assembling multiple micromixer units in series also enabled the immobilisation of different enzymes in separate units to carry out sequential reactions in a modular system. As a proof of concept, the solution product collected from long term biocatalysis was also tested in a direct formic acid fuel cell, which showed a promising prospect of integrating these two systems for a closed-loop energy generation system.

1. Introduction

Micromixer technologies have attracted significant research interests in the chemical and biological fields for applications such as chemical synthesis, RNA/DNA analysis, PCR amplification, and detection of chemical contents [1–3]. In particular, passive micromixers are simple to operate as enhanced mixing occurs following the change in structure along the channel length, allowing easy integration with other devices [1,4]. Various structures or features in the microchannel can be implemented to optimise the mixing efficiency, including Y or T shaped multi-input channels [5–7], interdigital channels [8–10], zig-zag channels [11], channels with staggered herringbone grooves [12], network of interconnecting channels defined by glass fibre strands [13], and also a combination of the different mixing units [14]. Furthermore, the introduction of a gas phase into the micromixer in a segmented gas–liquid flow has also been shown to enhance advection or mixing in the liquid [15]. Many researchers have started to report on the use of micromixers for gas–liquid dispersions as gas–liquid contacting is involved in many industrially relevant processes. The large gas–liquid interfacial areas due to the small dimensions of the microchannels can significantly improve the gas–liquid mass transfer rate, which is well suited for applications such as gas absorption. Yue *et al.* [16] and Hou *et al.* [17] investigated the mass transfer characteristics of micromixers with rectangular channel and arborescence channel respectively through the absorption of CO_2 gas into water and alkaline solutions. The volumetric mass transfer coefficients of both mixers were found to be at

* Corresponding authors at: Centre for Technology in Water and Wastewater, University of Technology Sydney, Ultimo, New South Wales 2007, Australia.
E-mail address: amir.razmjouchaharmahali@uts.edu.au (A. Razmjou).
[1] These authors contributed equally as first author.

https://doi.org/10.1016/j.cej.2021.130856
Received 5 March 2021; Received in revised form 7 June 2021; Accepted 12 June 2021
Available online 16 June 2021

least one or two orders of magnitude higher than that of traditional contactors such as bubble column and packed column [16,17]. Given the enhanced mass transfer performance of micromixers compared to traditional contactors, opportunities exist to implement micromixers for biocatalytic reactions involving a CO_2 gas phase and a liquid phase. An example applied in this study is the synthesis of formic acid via enzymatic cascade reaction of CO_2. CO_2 gas, along with a solvent, can be introduced into a micromixer where CO_2 is first hydrated to bicarbonate in a reaction catalysed by carbonic anhydrase (CA) [18,19]. This is then followed by a reduction reaction to formic acid catalysed by NADH-dependent formate dehydrogenase (FDH), which requires a redox cofactor (NADH) as the terminal electron donor [19–24]. In this reaction, the reduction of bicarbonate to formic acid is accompanied by the oxidation of NADH to NAD^+.

Changes to the microenvironment of an enzyme, such as pH and temperature, outside its optimal range can lead to a loss of bioactivity and even denaturation [25]. Therefore, enzyme immobilisation on a solid support is a popular strategy to enhance the stability of enzymes in operational and storage conditions [26–28]. Furthermore, enzyme immobilisation allows facile separation from the product, which improves the recyclability of enzymes [29]. In addition, immobilisation of multiple enzymes at adjacent positions (spatial immobilisation) also reduces the diffusion distance of intermediate product to the subsequent enzyme in the cascade reaction, which can improve the product yield [19]. Metal-organic frameworks (MOFs) have gained increasing interest over recent years as a platform for enzyme immobilisation. They are constructed from metal ions and multidentate ligands, which self-assemble through coordination bonds into 3D extended structures. A diverse range of MOFs has been synthesised and explored over the past two decades with exceptional properties such as high specific surface area, well-defined pores, and outstanding thermal and chemical stability, making them popular candidates for enzyme immobilisation [30]. Recently, Kang *et al.* [28] proposed an approach of immobilising proteins, enzymes, and DNA *in-situ* during the crystallisation process of MOFs, which encapsulates the biomacromolecules and also serves as an effective protective coating against harsh thermal and chemical treatments. This approach, known as biomineralisation, has since then been employed in several studies with different MOFs such as zeolitic imidazolate framework-8 (ZIF-8) [31,32], ZIF-90 [33], HKUST [34,35], MIL-53 [36,37], UiO-66-NH_2 [38] and NKMOF [39].

Among the numerous subclasses of MOF, ZIF-8 is the most popular MOF material used for *in-situ* encapsulation of enzymes due to its mild and biocompatible synthesis conditions [28]. This material has also been used in a broad range of applications, including gas separation [40,41], catalysis [31,42], biosensing [43], and adsorption of organic compounds [44]. It is constructed via the self-assembly of tetrahedrally-coordinated Zn^{2+} ions and 2-methylimidazole linkers, forming a highly crystalline microporous material with high thermal, chemical, and mechanical stability [45]. The imidazole group in ZIF-8 can act as a nucleophilic agent and react with CO_2 under an aqueous condition to form HCO_3^- [46]. Therefore, there is a synergistic effect of ZIF-8 and CA enzyme in the hydration reaction of CO_2 to bicarbonate. Zhang *et al.* [47] and Ren *et al.* [48] reported higher apparent catalytic activity of up to 22-folds for carbonic anhydrase encapsulated in ZIFs compared to their free counterpart. Furthermore, the activity of the FDH enzyme in the cascade reaction of CO_2 to formic acid can also be improved due to the higher concentration of HCO_3^- substrate produced [38]. Recently, Munirah *et al.* [43] found that for the case of a ZIF-8/enzyme *in-situ* thin film synthesised via biomineralisation, the enzymes are not fully encapsulated in ZIF-8 but are instead dispersed in the ZIF-8 matrix close to the surface. This is supported by the observation that a chemical inhibitor (chymotrypsin) which is larger than the ZIF-8 pore window can access and deactivate the enzymes [43]. ZIFs can also trap enzymes in the crystal defects that occur during the biomineralisation of MOF, which can provide alternative passageways for the movement of substrates larger than the ZIF-8 pore window to and from the enzymes [33,49–51]. This would allow for the movement of enzyme cofactor (NADH) to the FDH enzyme in the reduction reaction of bicarbonate to formic acid [38].

Although formic acid can be an intermediate product for subsequent enzymatic reactions to produce methanol as a liquid fuel, studies have shown that a bottleneck appears in the next reaction step catalysed by formaldehyde dehydrogenase due to the slow accumulation of formic acid [52,53]. Therefore, the question arises whether the formic acid product from biocatalysis can be utilised for other applications. Formic acid itself is a chemical of commercial interest as it can be used for tanning leather [54] and as a silage preservative [55]. Over the past two decades, several studies have also been conducted on direct formic acid fuel cells (DFAFC) utilising formic acid as a fuel. DFAFC exhibits several advantages over direct methanol fuel cell, such as small fuel crossover flux and high theoretical open circuit potential of 1.40 V compared to 1.21 V for direct methanol fuel cell [56]. Typically, formic acid oxidation on Pt-based catalysts proceeds through two pathway mechanisms. The desirable pathway is the dehydrogenation reaction of formic acid directly to CO_2, while the undesirable pathway is the dehydration reaction of formic acid that forms CO as a reaction intermediate [57]. The *in-situ* generated CO intermediate can readily adsorb onto the Pt surface and induce catalytic deactivation of the electrode, which impedes further fuel oxidation [58]. Wang *et al.* [59] found that the oxidative removal of adsorbed CO on Pt is initiated at 0.3 V for a Pt/C rotating disk electrode, due to the generation of adsorbed OH species originating from water dissociation. Therefore, it is undesirable to operate below this potential as the dehydration step acted solely as a site-blocking poison rather than a reaction intermediate.

In this paper, we demonstrate the use of a novel 3D printed micromixer with unique features (threaded channel) to enhance the mass transfer in the enzymatic cascade reaction of CO_2 to formic acid. Two enzymes, carbonic anhydrase and formate dehydrogenase, were co-immobilised via biomineralisation in a ZIF-8 thin film on the surface of the micromixer channel. The performance of the micromixer in terms of formic acid production rate was evaluated in comparison to a micromixer without threaded channel and a conventional bubble column as a benchmark. Furthermore, the effect of liquid flow rate as well as spatial (domino) immobilisation of enzymes on formic acid yield were also investigated. Lastly, as a proof of concept, the biocatalysis product collected from the micromixer was tested in a direct formic acid fuel cell to demonstrate that it is a viable fuel source for the fuel cell using commercial Pt/C catalyst, indicating the potential integration of these two catalytic systems for portable, green energy generation.

2. Experimental section

2.1. Materials

Zinc nitrate hexahydrate, 2-methylimidazole, tris(hydroxymethyl) aminomethane, dopamine hydrochloride, polyethyleneimine (MW = 800), hydrochloric acid, ethylenediaminetetraacetic acid (EDTA), reduced nicotinamide adenine dinucleotide (NADH), isopropyl alcohol (IPA), fluorescein isothiocyanate (FITC), atto 550 NHS ester, dimethyl sulfoxide (DMSO), sodium carbonate and sodium bicarbonate were purchased from Sigma Aldrich at the highest purity. Carbonic anhydrase from bovine erythrocytes (E.C. 4.2.1.1) with a specific activity of $\geq$ 2000 W-A units/mg protein and formate dehydrogenase from Candida boidinii (E.C. 1.2.1.2) with a specific activity of 5–15 units/mg protein were also purchased from Sigma Aldrich.

2.2. Micromixer fabrication

Additive manufacturing, in particular stereolithography (SLA) 3D printing, has shown great promise in the fabrication of microfluidic devices [60,61]. In this SLA printing method, a laser is used to cure and build solid parts from liquid resins [62]. All 3D printed parts in this

study were fabricated using a SLA 3D printer (Form2, Formlabs, USA) in Clear Resin V4 (RS-F2-GPCL-04). The parts were first drafted in SolidWorks 2018 x64 (Dassault Systèmes SolidWorks Corporation, Waltham, MA, USA), a commercially available CAD software, and then exported as .stl file, which is a proper file format for 3D printer software packages. Our channel has two inlets, one for buffer with NADH solution and one for CO_2 gas, as well as one outlet. The file is then imported into the Preform software for pre-processing of the printing procedure. 50 μm layer thickness was selected to make sure that the parts have enough quality and accuracy while auto support generation was used to create supports for proper attachment of the part to the build plate. When the printing process is completed, the parts were removed from the build plate carefully and washed three times with IPA thoroughly. The internal holes of the channels are 2.3 mm in diameter, which is proper for removing uncured resins. The threads in the channel are 0.77 mm in width and 0.35 mm in height. Lastly, the parts were post-cured in a UV-curing chamber.

2.3. PDA/PEI modification, ZIF-8/CA&FDH in-situ thin film and ZIF-8/CA&FDH in-situ particle synthesis

The micromixer channel was functionalised with PDA/PEI before the synthesis of ZIF-8 thin film. 2 mg/mL dopamine hydrochloride and 2 mg/mL polyethyleneimine were mixed in a Tris-HCl buffer solution (0.05 M, pH 8.5), which was then recirculated in the micromixer channel at 0.5 mL/min for 6 h. Subsequently, the channel was rinsed with Milli-Q water to remove excess chemicals. The ligand solution was prepared by mixing 0.168 g 2-methylimidazole (2 mmol) in 2.7 mL of Milli-Q water, in which 2.1 mg of carbonic anhydrase and 2.1 mg of formate dehydrogenase were added. In a separate solution, 0.008 g zinc nitrate hexahydrate (0.027 mmol) was mixed in 0.3 mL of Milli-Q water. Following this, the ligand-enzyme and metal precursor solutions were mixed and injected into the PDA/PEI modified micromixer channel using a syringe and left for an hour. The remaining precursor solution was collected for Bradford assay to determine the amount of enzyme loaded by subtracting it with the initial enzyme concentration. Prior to Bradford assay, the remaining precursor solution was added with an equal volume of EDTA (62.5 mM) as a chelating agent to release any enzymes encapsulated in the ZIF-8 particles.

ZIF-8/CA&FDH in-situ particles were prepared by mixing 2.7 mL of water containing 0.168 g 2-methylimidazole (2 mmol), 0.70 mg of CA, and 0.70 mg of FDH with 0.3 mL of water containing 0.008 g zinc nitrate hexahydrate (0.027 mmol). The solution was stirred overnight for 12 h. When the ZIF-8/enzyme particles have settled, the supernatant was collected for Bradford assay to determine the enzyme loading. The particles were centrifuged at 5000 rpm for 5 min and washed with Milli-Q water three times before being resuspended in Milli-Q water.

2.4. Characterisation of ZIF-8/CA&FDH thin film

The surface morphology of the micromixer was examined using field emission scanning electron microscopy (NanoSEM 230). Atomic force microscopy (AFM) measurements were conducted using Bruker Dimension ICON SPM with a scan size of 5 μm to determine the surface roughness. Contact angle measurements were conducted with Theta Optical Tensiometer from Biolin Scientific using the sessile drop method (One Attension software) with a drop size of 4 μL. The Alpha II FTIR spectrometer from Bruker Fourier equipped with a diamond ATR accessory was used to analyse the surface chemistry from wavenumber of 400 to 4000 cm^{-1}. XRD analysis was also carried out using Empyrean I (Malvern Panalytical) thin film XRD using 2 theta method from 5 to 40° with a step size of 0.025° and 100 s per step to obtain crystallographic data of the ZIF-8/CA&FDH thin film.

2.5. Enzyme labelling for fluorescence microscopy

The procedure for enzyme labelling used was based on our previous study with some modifications [43]. 4.5 mg of FITC was dissolved in 0.5 mL of DMSO, which was subsequently mixed with 7 mg of CA in 2 mL of sodium carbonate-bicarbonate buffer (50 mM, pH 9.2). In a separate vial, 50 μL of 2 mg/mL atto 550 NHS ester was added slowly into 7 mg of FDH prepared in 2 mL of sodium carbonate-bicarbonate buffer (50 mM, pH 9.2). Following this, the FITC-CA and atto 550-FDH mixtures were shaken at 300 rpm in darkness for 2 h. Subsequently, the unreacted enzymes were separated from the labelled enzymes by using Illustra NAP-25 column (GE Healthcare Life Sciences) eluted with Milli-Q water. The first band eluted contains the dye-labelled enzyme, which was collected and used for *in-situ* immobilisation in ZIF-8 thin film. Fluorescence microscopy imaging was conducted using IX53 Inverted Microscope from Olympus at 480 nm for the FITC labelled enzyme and 554 nm for the atto 550 labelled enzyme.

2.6. Enzyme activity assay and precipitation test of hydrated CO_2 to $CaCO_3$

20 mL Tris-HCl buffer (0.05 M, pH 7) containing 1 mM NADH was recirculated in the micromixer at different liquid flow rates of 0.5–3 mL/min. In the case of a long term experiment conducted where the product of biocatalysis was to be utilised in a formic acid fuel cell, 50 mL of Tris-HCl buffer containing 15 mM NADH was used instead. The experiments were all conducted in batch mode. CO_2 gas was introduced into the micromixer channel via another inlet at a flow rate of 0.3 mL/min controlled by a metering bellows sealed valve (Swagelok), which was connected to a buffer tank. A schematic drawing of the experimental setup is provided in Fig. 1A. For the bubble column, the ZIF-8/CA&FDH *in-situ* particles were added into 20 mL of buffer solution containing NADH in a sealed bottle, and CO_2 gas was bubbled at a flow rate of 0.3 mL/min from the bottom using a hypodermic needle (B Braun™). The length-to-diameter ratio of the bottle is 2. This value usually varies between 2 and 5 for bubble columns used in biochemical applications [63]. UV–Vis spectrophotometer (Cary 300, Agilent Technologies, Australia) was used to measure the concentration of NADH periodically in the reaction solution at a wavelength of 340 nm. The formic acid yield was calculated based on the amount of NADH consumed, as described in the literature [20].

$CaCO_3$ precipitation test was carried out to determine the amount of hydrated CO_2 present in the buffer solution, based on the procedure given by Hou *et al.* [18]. 0.2 g of $CaCl_2$ was dissolved in 5 mL of 0.5 M Tris-HCl buffer (pH 9.6), which was then mixed with the 20 mL Tris-HCl buffer solution containing hydrated CO_2. The mixture was left to precipitate for 5 min before filtering with a filter paper. The amount of $CaCO_3$ precipitated was measured by weighing.

3. Results and discussion

3.1. Principles of mixing

CO_2 gas and buffer solution containing the enzyme cofactor (NADH) were introduced into a micromixer via two separate inlets (Fig. 1A). The CA and FDH enzymes immobilised *in-situ* in ZIF-8 thin film on the micromixer channel reduce CO_2 to formic acid via a cascade reaction. This involves an initial hydration step of CO_2 to bicarbonate catalysed by CA enzyme, which is a zinc-based metalloenzyme. At the active site of CA, a zinc-bound hydroxide attacks CO_2 carbon to form metal-bound bicarbonate, which is then displaced by an external water molecule [64,65]. This is followed by a reduction reaction of bicarbonate to formic acid catalysed by NADH-dependent FDH in an aqueous environment [19,38]. The bicarbonate substrate and NADH bind to the active center of FDH comprised of amino acid residues, where NADH serves as the terminal electron donor in the redox reaction [66]. The formation of 1

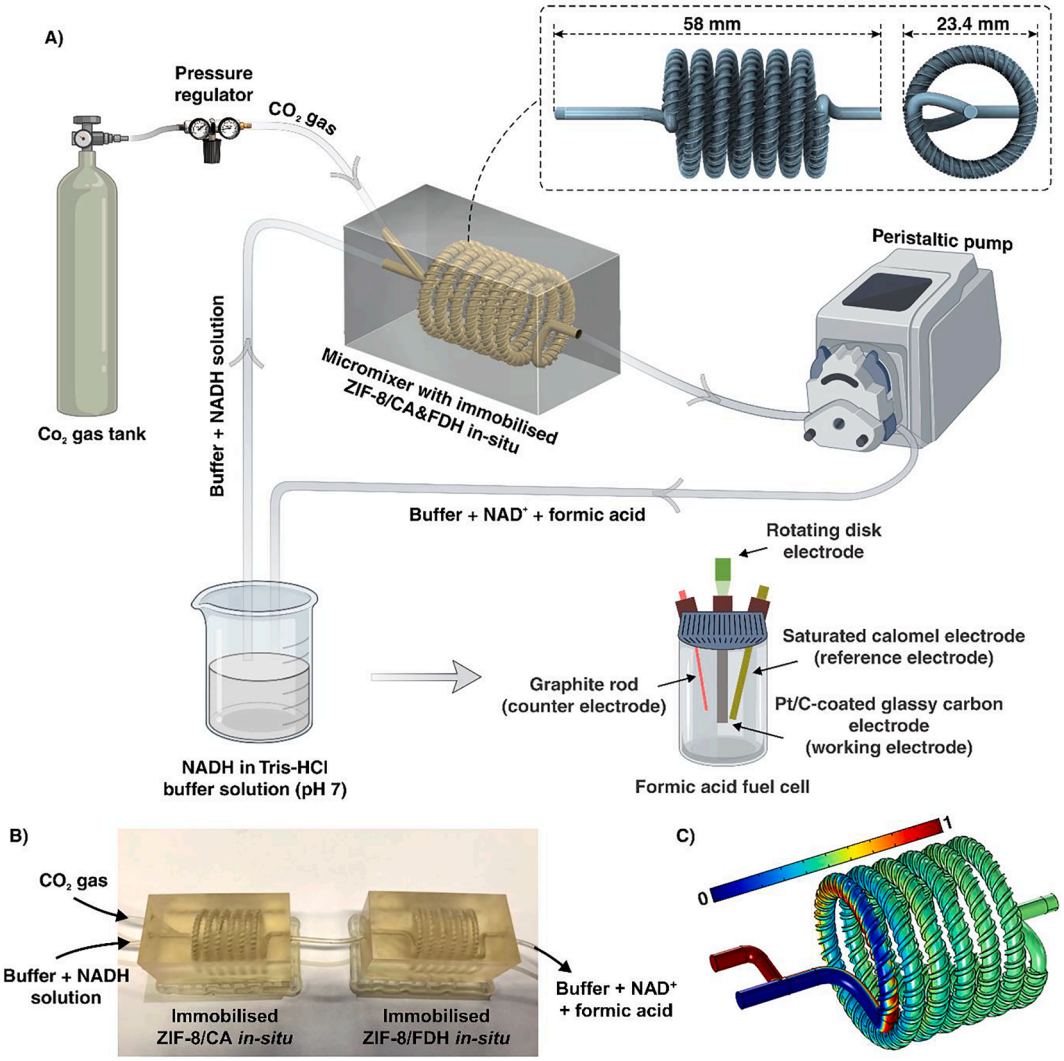

Fig. 1. A) Schematic illustration of biocatalytic micromixer setup used for the reduction of CO_2 to formic acid, with an enlarged view showing the 3D structure of the micromixer channel with threads to promote mixing. The intricate structures and features of the micromixer have been fabricated using 3D printing method. The product from biocatalysis was then utilised in a formic acid fuel cell for energy generation. B) The arrangement of two micromixers in series with CA and FDH enzymes immobilised in separate micromixers (domino immobilisation) for the enzymatic cascade reduction of CO_2. C) simulation results of concentration distribution of liquids within the micromixer (flow ratio is 1 to 1). Results show that ~ 100% mixing occurs at the channel outlet and sample becomes homogenous after 3 loops passing through the channel.

mol of formic acid requires 1 mol of NADH [19–24].

In order to increase the mixing index (MI) and volume of sample processed, a 3D structure was employed for the micromixer geometry. The third dimension of the micromixer structure allows the system to rapidly achieve and maintain a high MI over the length of the channel at both high and low Reynolds numbers [67]. In addition, the presence of threads in the micromixer channel increases the area of contact between the gas and liquid, which can enhance the mixing efficiency especially at low Reynolds number where diffusion is the dominant mixing mechanism. Hence, this device overcomes a common problem faced in many planar micromixers where they suffer from low mixing efficiency at the diffusion mixing regime. The designed threads around the channel also prevents particle settling by making the fluid flow from one side of the channel to the other. Furthermore, another benefit of this device over other typical micromixers is the uninterrupted presence of chaotic advection generated by Dean flow in the curved channels [68]. In contrast, the Dean flow is limited to a certain length and area due to the fabrication limitation of a planar micromixer. As the micromixer could achieve ~ 100% mixing efficiency across different Re at the early loops (Fig. 1C), the system is well suited for applications requiring controlled reaction of samples.

3.2. Characterisation of micromixer surface

SEM and AFM analysis were conducted to examine the surface morphology and roughness of the pristine, PDA/PEI modified, and ZIF-8/CA&FDH *in-situ* thin film on the micromixer surface (Fig. 2). The surface of the pristine micromixer is shown in Fig. 2A, which has a root mean square (RMS) surface roughness of 11.3 nm (Fig. 2B). The addition of dopamine hydrochloride and PEI formed a uniform layer of PDA/PEI on the micromixer surface due to a reaction between the amine group in PEI and catechol group in PDA (Fig. 2C), which can proceed through Michael addition or Schiff base reaction [69]. The surface roughness remained comparable to that of the pristine surface (Fig. 2D). Subsequently, the chelation of Zn metal ion by the catechol group in PDA enables the nucleation and growth of a highly intergrown thin film layer of ZIF-8 (Fig. 2E). There was an increase in surface roughness to 42.5 nm due to the presence of ZIF-8 microstructures (Fig. 2F). The micro surface roughness of ZIF-8 is not expected to have a significant effect on the bulk flow behaviour and mass transfer as the relative roughness (surface

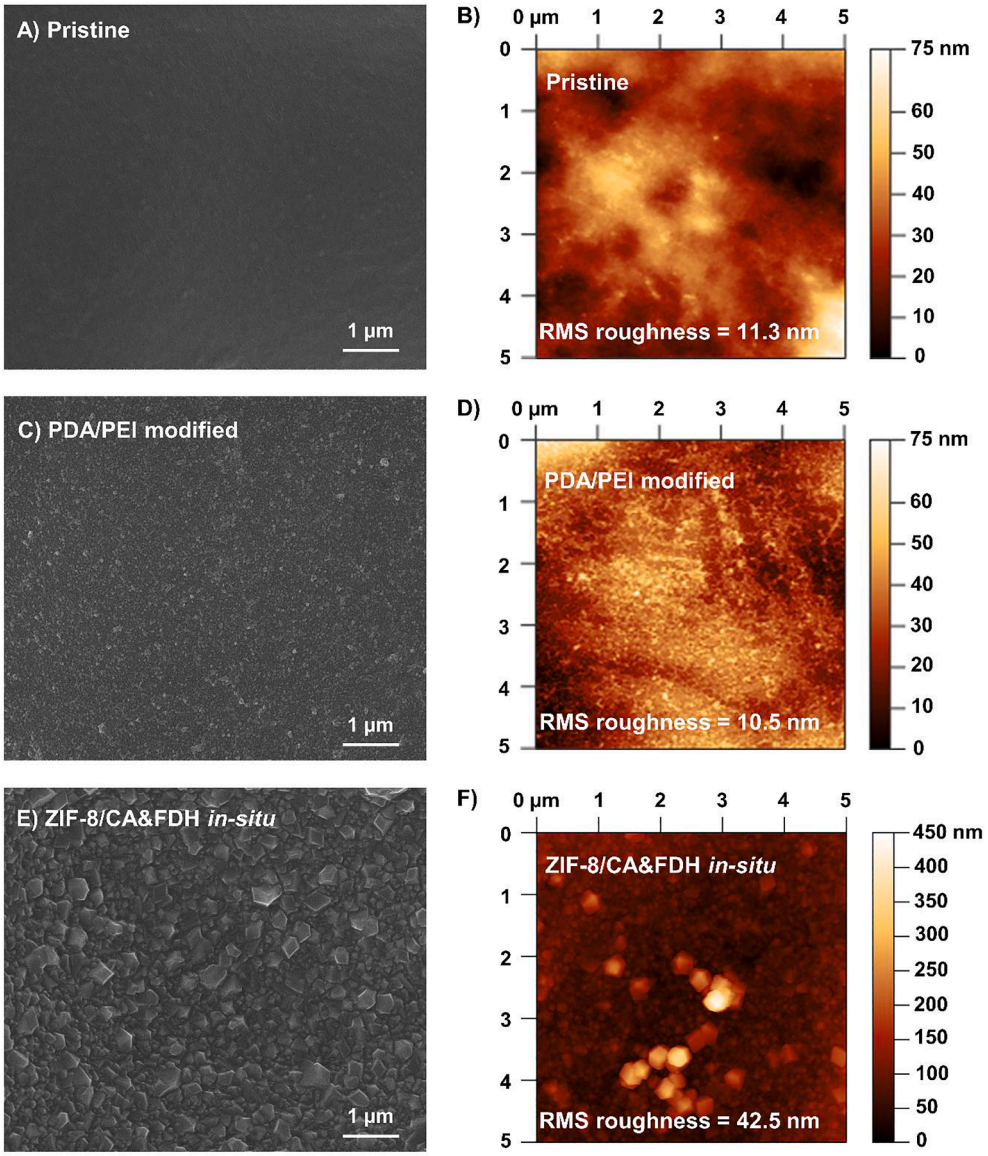

Fig. 2. A, C, E) SEM images of pristine, PDA/PEI modified, and ZIF-8/CA&FDH *in-situ* thin film showing the growth of a highly continuous ZIF-8/CA&FDH *in-situ* thin film on the PDA/PEI modified micromixer surface. B, D, F) AFM images of pristine, PDA/PEI modified, and ZIF-8/CA&FDH *in-situ* thin film on micromixer surface showing an increase in surface roughness due to the presence of ZIF-8 microstructures.

roughness/diameter of channel) is less than 0.00002 [70]. Zeng et al. [71] observed variations in the concentration profile due to rough structures in a microchannel, but for a relative roughness of 0.1 or higher. Two enzymes, carbonic anhydrase and formate dehydrogenase, were immobilised *in-situ* with the ZIF-8 thin film through a bio-mineralisation process as described in previous studies [28,43]. The presence of immobilised enzymes was further confirmed in fluorescence microscopy tests using fluorescence-labelled enzymes (Fig. 3). The water contact angle of the pristine micromixer surface showed that it is slightly hydrophobic (94.3° ± 4.1°) (Fig. 4A). Modification of the surface with PDA/PEI significantly improved the hydrophilicity, which reduced the water contact angle to 61.8° ± 4.2°. This is due to the abundance of amino groups present in PEI [72]. In most cases, a hydrophilic surface is favourable for the retention of enzyme activity during immobilisation as it reduces the hydrophobic interactions between enzyme and material that can cause conformational changes in enzymes [73]. The formation

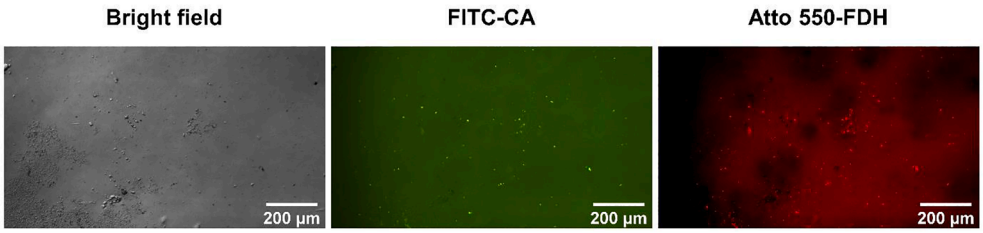

Fig. 3. Fluorescence microscopy images in bright field and fluorescence modes of FITC-CA and atto 550-FDH immobilised *in-situ* in the ZIF-8 thin film.

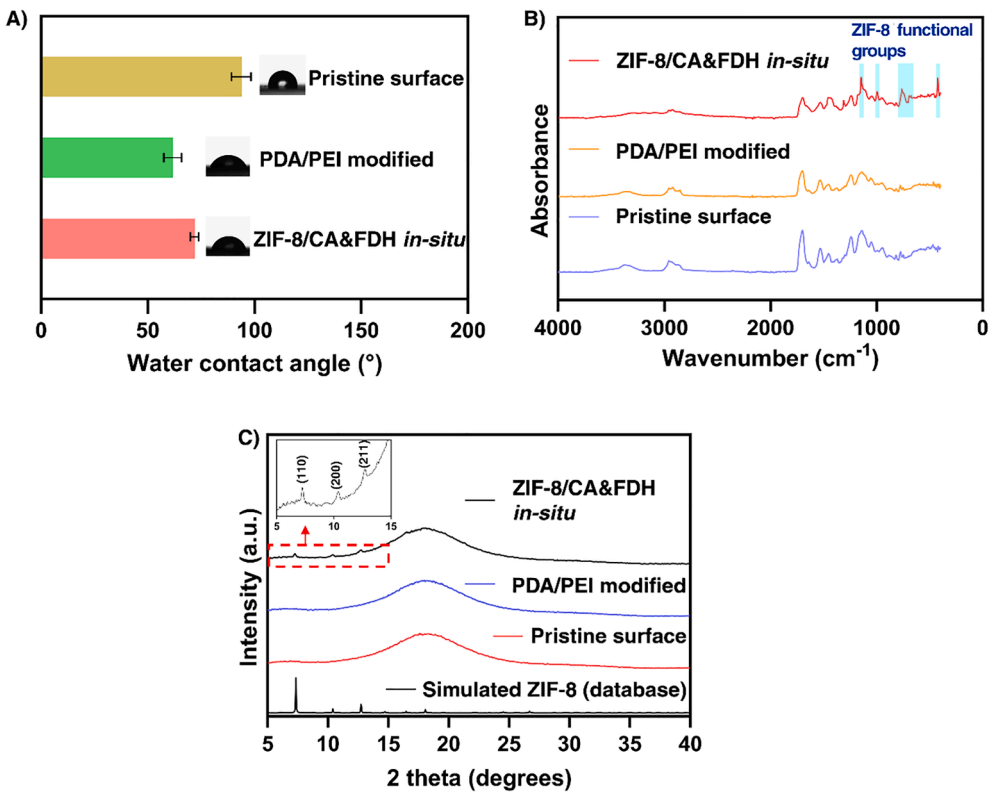

Fig. 4. A) Water contact angle measurement of pristine, PDA/PEI modified, and ZIF-8/CA&FDH *in-situ* thin film showing improved surface hydrophilicity following PDA/PEI modification. B) FTIR spectra of pristine, PDA/PEI modified, and ZIF-8/CA&FDH *in-situ* thin film with the absorption bands corresponding to the functional groups of ZIF-8 highlighted and C) XRD pattern of pristine, PDA/PEI modified, and ZIF-8/CA&FDH *in-situ* thin film confirming that the composite phase structure is ZIF-8.

of a ZIF-8/CA&FDH *in-situ* thin film on the PDA/PEI modified surface increased the water contact angle to 72.1° ± 1.5°. This is due to the increased surface roughness that can make the surface more hydrophobic, which is in agreement with the observation by Munirah *et al.* [43].

FTIR analysis was also conducted to examine the surface chemistry of the modified micromixer (Fig. 4B). Although there were no obvious differences between the FTIR spectra of PDA/PEI modified surface and pristine micromixer surface, the presence of PDA/PEI was previously observed from SEM and contact angle measurements. The broad absorption at 3200–3600 cm^{-1} can be attributed to the N–H/O–H stretching vibrations of PDA and PEI [74]. The formation of ZIF-8/CA&FDH *in-situ* thin film on the PDA/PEI modified surface revealed a characteristic absorption peak at 421 cm^{-1} from Zn-N stretching, indicating a reaction between Zn ions and nitrogen atoms of methylimidazole groups to form imidazolate [75]. In addition, new absorptions peaks were also observed at 660–800 cm^{-1} which corresponds to the plane bending of the imidazole ring [76]. Furthermore, the peaks at 995 cm^{-1} and 1146 cm^{-1} can be attributed to the aromatic C-N stretching mode [76].

XRD analysis of the ZIF-8/CA&FDH *in-situ* thin film confirms that the phase structure of the composite is ZIF-8 (Fig. 4C). Distinct peaks can be observed at 2θ positions of 7.4°, 10.4° and 12.7°, which are assigned to the 110, 200 and 211 planes, respectively [77]. The XRD pattern of the thin film is in good agreement with the simulated ZIF-8 pattern obtained from the database (PDF-4 database, ref ID: 00–062-1030).

3.3. Effect of liquid flow rate on biocatalytic activity

The effect of liquid flow rate on the biocatalytic activity in the micromixer was investigated. The CO_2 flow rate was fixed at 0.3 mL/min, as a relatively small adjustment was found to significantly change the two-phase flow pattern in the channel. For example, the channel was entirely filled with gas when the gas flow rate was increased to 0.5 mL/min at a liquid flow rate of 1 mL/min. Therefore, only the liquid flow rate was varied instead. The total enzyme loading in the ZIF-8/CA&FDH *in-situ* thin film was 0.68 mg. When the liquid flow rate was altered, the formic acid (FA) production rate after 6 h of catalysis increased from 0.37 $mol_{FA}/(kg_{enzyme}\ h)$ at 0.5 mL/min to 0.97 $mol_{FA}/(kg_{enzyme}\ h)$ at 1 mL/min; however, the production rate decreased to 0.70 $mol_{FA}/(kg_{enzyme}\ h)$ at 2 mL/min and 0.43 $mol_{FA}/(kg_{enzyme}\ h)$ at 3 mL/min (Fig. 5A). Detailed calculations of the formic acid production rate can be found in the Supporting Information (S1. Calculation of formic acid production rate). Therefore, 1 mL/min is the optimum liquid flow rate which corresponds to a Reynolds number of 8 and Dean number of 3 based on the superficial liquid velocity.

The two-phase flow pattern at the liquid flow rate of 0.5 mL/min was observed to be slug flow, which transitioned to bubbly flow at 1 mL/min (Fig. 5E). At liquid flow rates of 2 mL/min and above, the flow pattern was entirely bubbly flow. As the enzyme cascade reaction occurs in the aqueous environment [19], the lower overall biocatalytic activity observed at a flow rate of 0.5 mL/min compared to 1 mL/min could be due to the presence of long CO_2 gas slugs in the channel that hindered the reactions catalysed by CA and FDH enzymes. On the other hand, the flow rate also determines the residence time in the micromixer channel, and upon increasing the flow rate, the residence time decreases. The residence time at flow rates of 0.5 mL/min, 1 mL/min, 2 mL/min, and 3 mL/min are 3.7 min, 1.8 min, 0.9 min, and 0.6 min, respectively. While the mass transfer rate increases with increasing flow rate, this comes at the cost of a shorter residence time that can impair the conversion yield of products [78–80]. There may not be a complete, full contact between substrates and enzymes at flow rates higher than 2 mL/min, resulting in a decrease in formic acid production rate. This is similarly observed by Gong et al. [78] for the biocatalytic synthesis of isoquercitrin in a microreactor, where product yield decreased with a further increase in flow rate. In light of this, the optimum liquid flow rate of 1 mL/min was selected and used in this study.

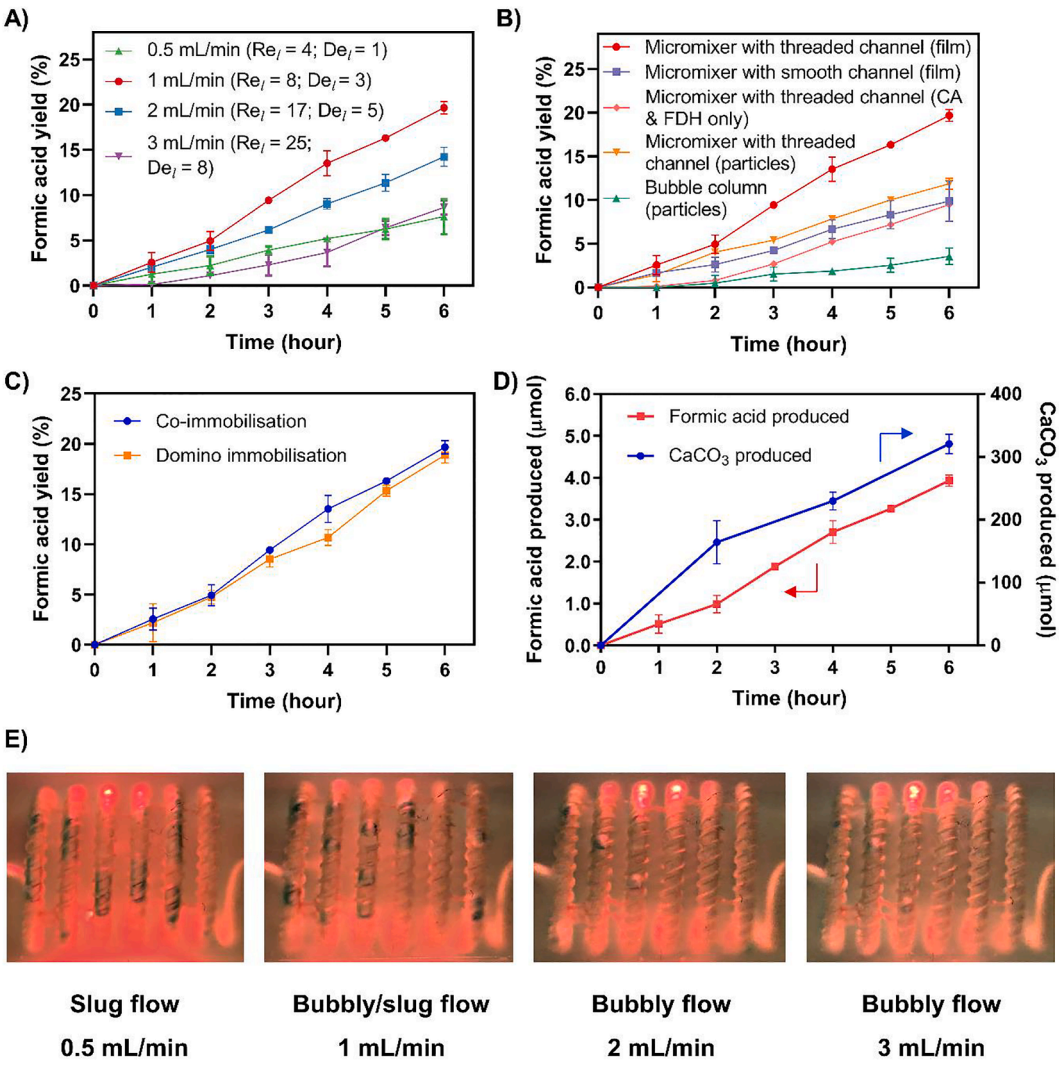

Fig. 5. A) Effect of liquid flow rate on catalytic performance. 1 mL/min for the fluid has been selected as the optimum flow rate and used for further experiments. B) Comparison of formic acid yield for biocatalytic micromixer with smooth and threaded channels in the presence or absence of ZIF-8, and benchmarking of catalytic performance with a bubble column using ZIF-8/CA&FDH particles. Formic acid yield in micromixer with threaded channel is higher than the unthreaded channel, indicating the significant effects of threads on enhancement of micromixer performance. The presence of ZIF-8 also resulted in increased catalytic activity due to the synergistic effect of ZIF-8 and CA enzyme. Moreover, the proposed micromixer has three times higher product yield compared to a conventional bubble column. C) Formic acid yield of CA&FDH enzyme cascade immobilised by co-immobilisation and domino immobilisation in the micromixer with the threaded channel. D) Amount of formic acid and $CaCO_3$ produced using the micromixer with the threaded channel. E) Two-phase flow patterns in the micromixer at different liquid flow rates of 0.5 mL/min, 1 mL/min, 2 mL/min and 3 mL/min revealing a transition from slug flow to bubbly flow at 1 mL/min.

3.4. Evaluation of micromixer performance with benchmarks

The performance of the micromixer with threads winding around the channel was compared to a similar micromixer with smooth channel to investigate the effect of threads on the mass transfer within the channel. The micromixer with smooth channel had the same 3D helical geometry as the micromixer with threaded channel, but without the threads. The total enzyme loading in the ZIF-8/CA&FDH thin film on the micromixers with threaded and smooth channels were 0.68 mg and 0.91 mg respectively, which corresponds to immobilisation yields (enzyme loaded/enzyme added) of 16% and 22%. As shown in Fig. 5B, the formic acid production rate for the micromixer with threaded channel was significantly higher at 0.97 $mol_{FA}/(kg_{enzyme}\ h)$ compared to the other case of 0.36 $mol_{FA}/(kg_{enzyme}\ h)$. This can be attributed to the improved mixing of gas and liquid in the microscale due to the presence of threads, which increased the mass transfer of the CO_2 substrate and intermediate product to the enzymes. Alam and Kim [81] found that a curved microchannel with rectangular grooves at the side walls provided better mixing performance with an increase in mixing index of up to 135% compared to a curved smooth channel. Furthermore, Stroock *et al.* [82] also determined that grooves positioned at an angle (slanted) to the flow direction resulted in a streamline with helicoidal shape, which may further improve mixing. They demonstrated that the use of micro-fabrication technology can allow for precise control of the surface patterning in the microchannel, which allows the flow behaviour to be tuned to maximise mixing.

In order to elucidate the influence of ZIF-8 on the CO_2 reduction reaction, CA and FDH enzymes were immobilised on the micromixer with the threaded channel in the absence of ZIF-8. The total enzyme loading was 0.56 mg, which corresponds to an immobilisation yield of 13%. The formic acid production rate after 6 h of catalysis was 0.56 $mol_{FA}/(kg_{enzyme}\ h)$, which is lower than the case with ZIF-8/CA&FDH thin film of 0.97 $mol_{FA}/(kg_{enzyme}\ h)$. The higher catalytic activity in the presence of ZIF-8 can be attributed to the contribution of ZIF-8 in the hydration reaction of CO_2. The imidazole group in ZIF-8 can act as a nucleophilic agent and react with CO_2 in an aqueous solution to form

bicarbonate, as follows [46,83]:

$$H_2O + mIm + CO_2 \rightleftharpoons mIm^+ + HCO_3^-(1)$$

Therefore, there is a synergistic effect of ZIF-8 and CA enzyme to enhance the CO_2 hydration rate. The increase in CO_2 hydration rate of CA enzyme with ZIF-8 was similarly reported by Ren et al. [48] and Zhang et al. [47], where the amount of CO_2 hydrated for CA@ZIF-8 composite was up to 22 times higher compared to CA enzyme alone. Therefore, CA enzyme in the presence of ZIF-8 provides a higher concentration of soluble HCO_3^- substrate to the FDH enzyme, resulting in the increased formic acid yield. This is also consistent with the observation in our previous study [38].

The micromixer performance was also compared to that of a simple bubble column as benchmark (Fig. 5B), where CO_2 gas was bubbled in a solution containing ZIF-8/CA&FDH particles. The CO_2 flow rate was 0.3 mL/min, similar to that used for the micromixer. The flow pattern in the column was observed to be bubbly flow. The total enzymes loaded in the particles was 1.2 mg, with an immobilisation yield of 87%. The biocatalytic performance of the bubble column with a formic acid production rate of 0.10 $mol_{FA}/(kg_{enzyme}\ h)$ was significantly lower than that of the micromixers. In comparison, the use of ZIF-8/CA&FDH particles in the micromixer with threaded channel showed a production rate of 0.33 $mol_{FA}/(kg_{enzyme}\ h)$. The lower CO_2 conversion observed for enzymes immobilised in ZIF-8 particles compared to ZIF-8 thin film could be due to a better contact with CO_2 for enzymes localised in the film at the threaded channel area where enhanced mixing occurs. As the characteristic dimension is drastically smaller in the micromixer compared to bubble column (2.3 mm diameter micromixer channel compared to 2.5 cm diameter column), the gas–liquid interfacial area and mass transfer rates are expected to be significantly higher for the micromixer. Yue *et al.* [16] determined that a microchannel contactor can provide a liquid side volumetric mass transfer coefficient and gas–liquid interfacial area of at least one or two orders of magnitude higher than other gas–liquid contactors, including bubble column and packed column. This allows the cascade reaction of CO_2 to formic acid to proceed at a faster rate in the micromixer compared to the bubble column. Apart from CO_2 reduction, microchannel contactors have also been used for other gas–liquid reactions, such as halogenation and hydrogenation reactions [84–86]. The space–time yields in a gas–liquid microchannel for direct fluorination of toluene were found to be orders to magnitude higher than that of a bubble column, as miniaturisation allowed fluorination to proceed in a few seconds rather than a few hours [84].

3.5. Effect of domino immobilisation for enzymatic cascade

The effect of immobilising the CA and FDH enzymes in separate micromixers rather than co-immobilising the two enzymes in one micromixer was evaluated. As individual units of the micromixers can be connected in series easily through a tube (Fig. 1B), the CO_2 substrate can first be introduced to the CA enzyme immobilised in the first micromixer, and then intermediate product (bicarbonate) may continue downstream to the second micromixer with FDH enzyme for further reduction to formic acid. This enables a directional reaction sequence that follows the fluid flow. The amount of enzyme immobilised in each micromixer were 0.40 mg of CA and 0.55 mg of FDH, which corresponds to an enzyme immobilisation yield of 31.7% and 44.0% respectively.

As shown in Fig. 5C, the formic acid yield observed for co-immobilisation and domino immobilisation of enzymes were quite similar. Further CO_2 hydration tests conducted on the micromixer with only the CA enzyme showed that the bicarbonate produced is two orders of magnitude higher than that of formic acid (Fig. 5D), indicating that the rate-limiting step occurs in the catalysis step of the FDH enzyme. This is supported by the observation by Zhu *et al.* [53] who found that the cascade bottleneck lies with the redox reaction catalysed by FDH enzyme. Oxidoreductases such as FDH function in the presence of redox cofactors like NADH as the reducing power or electron donor to the biocatalysis reaction [87,88]. The substrate and NADH bind to the active site of FDH where electron exchange takes place, reducing bicarbonate to formic acid while NADH is oxidised to NAD^+ [19]. As the efficiency of formic acid conversion is determined by electron transfer, a possible method to improve the reduction reaction is the application of bioelectrocatalysis [89]. The cathode can supply electrons for an enhanced reduction reaction directly by enhancing the bioelectrocatalysis of FDH enzyme, or by increasing the availability of reduced NADH through regeneration [87,90,91]. Therefore, it is envisioned that the incorporation of microelectrodes in the micromixer for bioelectrocatalysis can improve the formic acid yield, which is feasible as it has been done in other similar applications such as an electrochemical microreactor for NADH regeneration [92].

Although the implementation of domino immobilisation did not yield any benefits in this case, the flexibility of the micromixers in which individual units can be easily assembled and disassembled is still of great interest because different types of enzymes can be immobilised at predefined locations to carry out reactions with a specific reaction order. Thus, a modular device where each module is doing its specific function while integrated can be fabricated and designed. These devices are also fabricated via 3D printing method, which allows rapid evaluation of an ideated solution. The fabrication of each device, from designing a part to performing the post-processing of the 3D printed channel, takes only less than 4 h which elucidates the huge potential of 3D printing in the fabrication of microfluidic devices. Apart from CO_2 reduction, it is envisioned that these devices can also be applied for analytical and diagnostic applications, such as quantification of lactose in milk [93].

3.6. Direct formic acid fuel cell

A long term biocatalysis experiment was conducted over 4 days in batch mode. The formic acid conversion rate started to plateau after 3 days and reached 91% after 4 days, which corresponds to a concentration of 13 mM in the Tris-HCl buffer solution (Fig. 6A). The product from the biocatalysis experiment containing formic acid and impurities (Tris-HCl, bicarbonate, NADH/NAD^+) was then tested for electrochemical formic acid oxidation (FAO) reactions, which is a half-reaction in formic acid fuel cells. In this test, we drop-cast commercial Pt/C ink with a catalyst loading of 0.25 mg cm^{-2} on a glassy carbon electrode (GCE) and employ this as the working electrode alongside a graphite rod as the counter and saturated calomel electrode (SCE) as the reference. Our bulk electrolysis results (Fig. 6B) at 0.4 V vs SCE reveal much more enhanced steady-state current density (~0.02 mA cm^{-2}) in electrolyte solution containing 0.1 M $HClO_4$ and products from biocatalysis experiments. Note that we apply electrolysis at this potential as the potential is higher than what is reported for Pt oxidation [59]. We conclude that this current density is arising from FAO and not water oxidation, as the background 0.1 M $HClO_4$ is displaying negligible current density at the same applied potential. There is a decline in formic acid oxidation activity over time as indicated by the slight decrease in current density in Fig. 6B. This may arise from the decreasing formic acid concentration as reactants are being consumed over the course of the reaction, as well as possible poisoning of the catalyst arising from CO generation and impurities present in the electrolyte solution [57,94]. While the concentration of formic acid in the biocatalysis product is limited (and hence the low current density attained), the collective results show the prospect of integrating both the systems to develop a close loop CO_2 to the energy generation system. The addition of a second metal or modifier such as Bi, Pb, Pd, or Au will likely enhance the activity of Pt catalyst towards formic acid oxidation [59,95–97]. This is believed to be due to the breach of platinum ensembles (continuous neighbouring atomic sites) that inhibits the CO poisoning effect, which can be further explored in future studies.

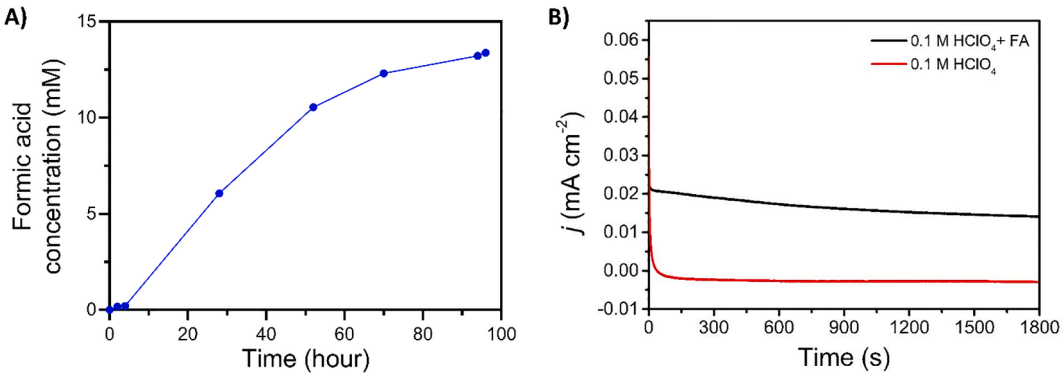

Fig. 6. A) Formic acid concentration in the Tris-HCl buffer solution during long term biocatalysis experiment over 4 days. B) Chronoamperometric *i*-t curve at 0.4 V vs SCE showing the formic acid oxidation using Pt/C catalyst.

4. Conclusion

A novel 3D micromixer with a helical shaped, threaded channel can improve the mixing and hence mass transfer of substrates to two enzymes, carbonic anhydrase (CA) and formate dehydrogenase (FDH), which are immobilised in-situ in ZIF-8 thin film on the channel. CO_2 and a buffer solution containing NADH were introduced into the micromixer via separate inlets, where CO_2 was initially hydrated to bicarbonate by CA enzyme, followed by reduction to formic acid by FDH enzyme in a cascade reaction. The liquid flow rate (1 mL/min; $Re_l = 8$; $De_l = 3$) at which the two-phase flow pattern transitioned from slug flow to bubbly flow was found to yield the highest product conversion rate. The benefit of threads in the micromixer channel was clear, as the formic acid production rate was found to increase to 0.97 $mol_{FA}/(kg_{enzyme}\ h)$ from 0.36 $mol_{FA}/(kg_{enzyme}\ h)$ for a smooth channel. In addition, benchmarking with a conventional bubble column also showed a higher formic acid yield for the micromixer with threaded channel by three folds. As individual enzymes can be immobilised in separate micromixer units and assembled in series, this also enabled reactions with a specific reaction order to take place. We also present an initial proof of concept for the development of a closed-loop CO_2 to energy generation system, by using the product from biocatalysis in a direct formic acid fuel cell. A steady-state current density of approximately 0.02 mA cm^{-2} was observed arising from formic acid oxidation, albeit low due to the low formic acid concentration, nevertheless shows the prospect of integrating these two systems for green energy generation.

Declaration of Competing Interest

The authors declare that they have no known competing financial interests or personal relationships that could have appeared to influence the work reported in this paper.

Acknowledgements

Vicki Chen acknowledge support from the Australian Research Council (ARC) (DP150104485, DP180103874). The authors acknowledge the facilities and the scientific and technical assistance of Microscopy Australia at the Electron Microscope Unit (EMU) and Solid State & Elemental Analysis Unit (SSEAU) within the Mark Wainwright Analytical Centre (MWAC) at UNSW Sydney.

Appendix A. Supplementary data

Supplementary data to this article can be found online at https://doi.org/10.1016/j.cej.2021.130856.

References

[1] C.-T. Wang, Y.-C. Hu, T.-Y. Hu, Biophysical micromixer, Sensors 9 (2009) 5379–5389.
[2] G.S. Jeong, S. Chung, C.-B. Kim, S.-H. Lee, Applications of micromixing technology, Analyst 135 (2010) 460–473.
[3] M. Rasouli, A. Abouei Mehrizi, M. Goharimanesh, A. Lashkaripour, S. Razavi Bazaz, Multi-criteria optimization of curved and baffle-embedded micromixers for bio-applications, Chemical Engineering and Processing - Process Intensification, 132 (2018) 175-186.
[4] S. Razavi Bazaz, H.A. Amiri, S. Vasilescu, A. Abouei Mehrizi, D. Jin, M. Miansari, M. Ebrahimi Warkiani, Obstacle-free planar hybrid micromixer with low pressure drop, Microfluidics and Nanofluidics, 24 (2020) 61.
[5] D. Gobby, P. Angeli, A. Gavriilidis, Mixing characteristics of T-type microfluidic mixers, J. Micromech. Microeng. 11 (2001) 126.
[6] S. Razavi Bazaz, A.H. Hazeri, O. Rouhi, A.A. Mehrizi, D. Jin, M.E. Warkiani, Volume-preserving strategies to improve the mixing efficiency of serpentine micromixers, J. Micromech. Microeng. 30 (2020), 115022.
[7] Y.S.S. Wan, J.L.H. Chau, A. Gavriilidis, K.L. Yeung, Design and fabrication of zeolite-based microreactors and membrane microseparators, Microporous Mesoporous Mater. 42 (2001) 157–175.
[8] V. Hessel, S. Hardt, H. Löwe, F. Schönfeld, Laminar mixing in different interdigital micromixers: I, Experimental characterization, AIChE Journal 49 (2003) 566–577.
[9] X. Chen, K.L. Yeung, Chemical Engineering Process Miniaturisation for Chemical Production and Material Manufacture, HKIE Transactions 19 (2012) 29–33.
[10] T.N. Ng, X. Chen, K.L. Yeung, Direct manipulation of particle size and morphology of ordered mesoporous silica by flow synthesis, RSC Adv. 5 (2015) 13331–13340.
[11] W. Jeon, C.B. Shin, Design and simulation of passive mixing in microfluidic systems with geometric variations, Chem. Eng. J. 152 (2009) 575–582.
[12] D. Hassell, W. Zimmerman, Investigation of the convective motion through a staggered herringbone micromixer at low Reynolds number flow, Chem. Eng. Sci. 61 (2006) 2977–2985.
[13] K. He, W. Han, K.L. Yeung, Preparation and performance of catalytic MOFs in microreactor, J. Taiwan Inst. Chem. Eng. 98 (2019) 85–93.
[14] S.R. Bazaz, A.A. Mehrizi, S. Ghorbani, S. Vasilescu, M. Asadnia, M.E. Warkiani, A hybrid micromixer with planar mixing units, RSC Adv. 8 (2018) 33103–33120.
[15] A. Günther, M. Jhunjhunwala, M. Thalmann, M.A. Schmidt, K.F. Jensen, Micromixing of miscible liquids in segmented gas− liquid flow, Langmuir 21 (2005) 1547–1555.
[16] J. Yue, G. Chen, Q. Yuan, L. Luo, Y. Gonthier, Hydrodynamics and mass transfer characteristics in gas–liquid flow through a rectangular microchannel, Chem. Eng. Sci. 62 (2007) 2096–2108.
[17] J. Hou, G. Qian, X. Zhou, Gas–liquid mixing in a multi-scale micromixer with arborescence structure, Chem. Eng. J. 167 (2011) 475–482.
[18] J. Hou, M.Y. Zulkifli, M. Mohammad, Y. Zhang, A. Razmjou, V. Chen, Biocatalytic gas-liquid membrane contactors for CO2 hydration with immobilized carbonic anhydrase, J. Membr. Sci. 520 (2016) 303–313.
[19] S. Gao, M. Mohammad, H.-C. Yang, J. Xu, K. Liang, J. Hou, V. Chen, Janus Reactors with Highly Efficient Enzymatic CO2 Nanocascade at Air-Liquid Interface, ACS Appl. Mater. Interfaces 9 (2017) 42806–42815.
[20] Y. Lu, Z.-Y. Jiang, S.-W. Xu, H. Wu, Efficient conversion of CO2 to formic acid by formate dehydrogenase immobilized in a novel alginate–silica hybrid gel, Catal. Today 115 (2006) 263–268.
[21] S. Ikeyama, Y. Amao, An Artificial Co-enzyme Based on the Viologen Skeleton for Highly Efficient CO2 Reduction to Formic Acid with Formate Dehydrogenase, ChemCatChem 9 (2017) 833–838.
[22] X. Ji, Z. Su, P. Wang, G. Ma, S. Zhang, Tethering of nicotinamide adenine dinucleotide inside hollow nanofibers for high-yield synthesis of methanol from carbon dioxide catalyzed by coencapsulated multienzymes, ACS Nano 9 (2015) 4600–4610.
[23] P.K. Addo, R.L. Arechederra, A. Waheed, J.D. Shoemaker, W.S. Sly, S.D. Minteer, Methanol production via bioelectrocatalytic reduction of carbon dioxide: role of

carbonic anhydrase in improving electrode performance, Electrochem. Solid-State Lett. 14 (2011) E9–E13.
[24] Y. Wang, M. Li, Z. Zhao, W. Liu, Effect of carbonic anhydrase on enzymatic conversion of CO2 to formic acid and optimization of reaction conditions, J. Mol. Catal. B Enzym. 116 (2015) 89–94.
[25] H. Neurath, J.P. Greenstein, F.W. Putnam, J.A. Erickson, The chemistry of protein denaturation, Chem. Rev. 34 (1944) 157–265.
[26] R.A. Sheldon, S. van Pelt, Enzyme immobilisation in biocatalysis: why, what and how, Chemical Society Reviews 42 (2013) 6223–6235.
[27] U. Hanefeld, L. Cao, E. Magner, Enzyme immobilisation: fundamentals and application, Chem. Soc. Rev. 42 (2013) 6211–6212.
[28] K. Liang, R. Ricco, C.M. Doherty, M.J. Styles, S. Bell, N. Kirby, S. Mudie, D. Haylock, A.J. Hill, C.J. Doonan, Biomimetic mineralization of metal-organic frameworks as protective coatings for biomacromolecules, Nat. Commun. 6 (2015) 7240.
[29] X. Lian, Y. Fang, E. Joseph, Q. Wang, J. Li, S. Banerjee, C. Lollar, X. Wang, H.-C. Zhou, Enzyme–MOF (metal–organic framework) composites, Chem. Soc. Rev. 46 (2017) 3386–3401.
[30] J. Mehta, N. Bhardwaj, S.K. Bhardwaj, K.-H. Kim, A. Deep, Recent advances in enzyme immobilization techniques: Metal-organic frameworks as novel substrates, Coord. Chem. Rev. 322 (2016) 30–40.
[31] W.-H. Chen, M. Vázquez-González, A. Zoabi, R. Abu-Reziq, I. Willner, Biocatalytic cascades driven by enzymes encapsulated in metal–organic framework nanoparticles, Nat. Catal. 1 (2018) 689–695.
[32] X. Wu, J. Ge, C. Yang, M. Hou, Z. Liu, Facile synthesis of multiple enzyme-containing metal–organic frameworks in a biomolecule-friendly environment, Chem. Commun. 51 (2015) 13408–13411.
[33] F.-K. Shieh, S.-C. Wang, C.-I. Yen, C.-C. Wu, S. Dutta, L.-Y. Chou, J.V. Morabito, P. Hu, M.-H. Hsu, K.C.-W. Wu, Imparting functionality to biocatalysts via embedding enzymes into nanoporous materials by a de novo approach: size-selective sheltering of catalase in metal–organic framework microcrystals, J. Am. Chem. Soc. 137 (2015) 4276–4279.
[34] Y. Li, L. Wen, T. Tan, Y. Lv, Sequential co-immobilization of enzymes in metal-organic frameworks for efficient biocatalytic conversion of adsorbed CO2 to formate, Front. Bioeng. Biotechnol. 7 (2019) 394.
[35] R. Zhang, L. Wang, J. Han, J. Wu, C. Li, L. Ni, Y. Wang, Improving laccase activity and stability by HKUST-1 with cofactor via one-pot encapsulation and its application for degradation of bisphenol A, Journal of hazardous materials 383 (2020), 121130.
[36] V. Gascón, E. Castro-Miguel, M. Díaz-García, R.M. Blanco, M. Sanchez-Sanchez, In situ and post-synthesis immobilization of enzymes on nanocrystalline MOF platforms to yield active biocatalysts, J. Chem. Technol. Biotechnol. 92 (2017) 2583–2593.
[37] A. Samui, S.K. Sahu, One-pot synthesis of microporous nanoscale metal organic frameworks conjugated with laccase as a promising biocatalyst, New J. Chem. 42 (2018) 4192–4200.
[38] M. Chai, A. Razmjou, V. Chen, Metal-organic-framework protected multi-enzyme thin-film for the cascade reduction of CO2 in a gas-liquid membrane contactor, J. Membr. Sci. 118986 (2021).
[39] H. An, J. Song, T. Wang, N. Xiao, Z. Zhang, P. Cheng, H. Huang, S. Ma, Y. Chen, Metal-Organic Framework Disintegrants: A New Generation of Enzyme Preparation Platforms with Boosted Activity, Angew. Chem. Int. Ed. (2020).
[40] Q. Song, S. Nataraj, M.V. Roussenova, J.C. Tan, D.J. Hughes, W. Li, P. Bourgoin, M. A. Alam, A.K. Cheetham, S.A. Al-Muhtaseb, Zeolitic imidazolate framework (ZIF-8) based polymer nanocomposite membranes for gas separation, Energy Environ. Sci. 5 (2012) 8359–8369.
[41] M.J.C. Ordonez, K.J. Balkus Jr, J.P. Ferraris, I.H. Musselman, Molecular sieving realized with ZIF-8/Matrimid® mixed-matrix membranes, J. Membr. Sci. 361 (2010) 28–37.
[42] C.-H. Kuo, Y. Tang, L.-Y. Chou, B.T. Sneed, C.N. Brodsky, Z. Zhao, C.-K. Tsung, Yolk–shell nanocrystal@ ZIF-8 nanostructures for gas-phase heterogeneous catalysis with selectivity control, J. Am. Chem. Soc. 134 (2012) 14345–14348.
[43] M. Mohammad, A. Razmjou, K. Liang, M. Asadnia, V. Chen, Metal–Organic-Framework-Based Enzymatic Microfluidic Biosensor via Surface Patterning and Biomineralization, ACS Appl. Mater. Interfaces 11 (2018) 1807–1820.
[44] D. Wang, Z. Li, J. Zhou, H. Fang, X. He, P. Jena, J.-B. Zeng, W.-N. Wang, Simultaneous detection and removal of formaldehyde at room temperature: Janus Au@ ZnO@ ZIF-8 nanoparticles, Nano-micro letters 10 (2018) 4.
[45] D. Zou, D. Liu, J. Zhang, From Zeolitic Imidazolate Framework-8 to Metal-Organic Frameworks (MOF s): Representative Substance for the General Study of Pioneering MOF Applications, Energy & Environmental Materials 1 (2018) 209–220.
[46] Y. Zhang, H. Wang, J. Liu, J. Hou, Y. Zhang, Enzyme-embedded metal–organic framework membranes on polymeric substrates for efficient CO 2 capture, J. Mater. Chem. A 5 (2017) 19954–19962.
[47] S. Zhang, M. Du, P. Shao, L. Wang, J. Ye, J. Chen, J. Chen, Carbonic anhydrase enzyme-MOFs composite with a superior catalytic performance to promote CO2 absorption into tertiary amine solution, Environ. Sci. Technol. 52 (2018) 12708–12716.
[48] S. Ren, Y. Feng, H. Wen, C. Li, B. Sun, J. Cui, S. Jia, Immobilized carbonic anhydrase on mesoporous cruciate flower-like metal organic framework for promoting CO2 sequestration, Int. J. Biol. Macromol. 117 (2018) 189–198.
[49] X. Wu, C. Yang, J. Ge, Green synthesis of enzyme/metal-organic framework composites with high stability in protein denaturing solvents, Bioresources and bioprocessing 4 (2017) 24.
[50] Y. Pan, H. Li, J. Farmakes, F. Xiao, B. Chen, S. Ma, Z. Yang, How do enzymes orient when trapped on metal–organic framework (MOF) surfaces? J. Am. Chem. Soc. 140 (2018) 16032–16036.
[51] F.-S. Liao, W.-S. Lo, Y.-S. Hsu, C.-C. Wu, S.-C. Wang, F.-K. Shieh, J.V. Morabito, L.-Y. Chou, K.C.-W. Wu, C.-K. Tsung, Shielding against unfolding by embedding enzymes in metal–organic frameworks via a de novo approach, J. Am. Chem. Soc. 139 (2017) 6530–6533.
[52] J. Luo, A.S. Meyer, R.V. Mateiu, M. Pinelo, Cascade catalysis in membranes with enzyme immobilization for multi-enzymatic conversion of CO2 to methanol, New Biotechnol. 32 (2015) 319–327.
[53] D. Zhu, S. Ao, H. Deng, M. Wang, C. Qin, J. Zhang, Y. Jia, P. Ye, H. Ni, Ordered Coimmobilization of a Multienzyme Cascade System with a Metal Organic Framework in a Membrane: Reduction of CO2 to Methanol, ACS Appl. Mater. Interfaces 11 (2019) 33581–33588.
[54] H. Endres, F. Leppmeier, H. Erdmann, Tanning process, in, Google Patents (1970).
[55] J. Derbyshire, C. Gordon, D. Waldo, Formic acid as a silage preservative for milking cows, J. Dairy Sci. 59 (1976) 278–287.
[56] X. Yu, P.G. Pickup, Recent advances in direct formic acid fuel cells (DFAFC), Journal of Power Sources 182 (2008) 124–132.
[57] C. Rice, S. Ha, R. Masel, P. Waszczuk, A. Wieckowski, T. Barnard, Direct formic acid fuel cells, J. Power Sources 111 (2002) 83–89.
[58] Y.M. Asal, I.M. Al-Akraa, A.M. Mohammad, M.S. El-Deab, Design of efficient bimetallic Pt–Au nanoparticle-based anodes for direct formic acid fuel cells, International Journal of Hydrogen Energy 44 (2019) 3615–3624.
[59] X. Wang, J.-M. Hu, I.-M. Hsing, Electrochemical investigation of formic acid electro-oxidation and its crossover through a Nafion® membrane, J. Electroanal. Chem. 562 (2004) 73–80.
[60] S. Razavi Bazaz, O. Rouhi, M.A. Raoufi, F. Ejeian, M. Asadnia, D. Jin, M. Ebrahimi Warkiani, 3D Printing of Inertial Microfluidic Devices, Sci. Rep. 10 (2020) 5929.
[61] M.S. Syed, F. Mirakhorli, C. Marquis, R.A. Taylor, M.E. Warkiani, Particle movement and fluid behavior visualization using an optically transparent 3D-printed micro-hydrocyclone, Biomicrofluidics 14 (2020), 064106.
[62] J. Shrestha, M. Ghadiri, M. Shanmugavel, S. Razavi Bazaz, S. Vasilescu, L. Ding, M. Ebrahimi Warkiani, A rapidly prototyped lung-on-a-chip model using 3D-printed molds, Organs-on-a-Chip, 1 (2019) 100001.
[63] N. Kantarci, F. Borak, K.O. Ulgen, Bubble column reactors, Process Biochem. 40 (2005) 2263–2283.
[64] S. Lindskog, Structure and mechanism of carbonic anhydrase, Pharmacol. Ther. 74 (1997) 1–20.
[65] G.P. Miscione, M. Stenta, D. Spinelli, E. Anders, A. Bottoni, New computational evidence for the catalytic mechanism of carbonic anhydrase, Theor. Chem. Acc. 118 (2007) 193–201.
[66] Y. Amao, Formate dehydrogenase for CO2 utilization and its application, J. CO2 Util. 26 (2018) 623–641.
[67] S.A. Vasilescu, S.R. Bazaz, D. Jin, O. Shimoni, M.E. Warkiani, 3D printing enables the rapid prototyping of modular microfluidic devices for particle conjugation, Appl. Mater. Today 20 (2020), 100726.
[68] F. Jiang, K.S. Drese, S. Hardt, M. Küpper, F. Schönfeld, Helical flows and chaotic mixing in curved micro channels, AIChE J. 50 (2004) 2297–2305.
[69] Y. Lv, H.-C. Yang, H.-Q. Liang, L.-S. Wan, Z.-K. Xu, Nanofiltration membranes via co-deposition of polydopamine/polyethylenimine followed by cross-linking, J. Membr. Sci. 476 (2015) 50–58.
[70] G. Celata, M. Cumo, S. McPhail, G. Zummo, Characterization of fluid dynamic behaviour and channel wall effects in microtube, Int. J. Heat Fluid Flow 27 (2006) 135–143.
[71] Y. Zeng, T. Lee, P. Yu, H. Low, Effect of surface roughness on mass transfer in a flat-plate microchannel bioreactor, Mod. Phys. Lett. B 19 (2005) 1559–1562.
[72] H.-C. Yang, K.-J. Liao, H. Huang, Q.-Y. Wu, L.-S. Wan, Z.-K. Xu, Mussel-inspired modification of a polymer membrane for ultra-high water permeability and oil-in-water emulsion separation, J. Mater. Chem. A 2 (2014) 10225–10230.
[73] J.N. Talbert, J.M. Goddard, Enzymes on material surfaces, Colloids Surf., B 93 (2012) 8–19.
[74] G. Zin, J. Wu, K. Rezzadori, J.C.C. Petrus, M. Di Luccio, Q. Li, Modification of hydrophobic commercial PVDF microfiltration membranes into superhydrophilic membranes by the mussel-inspired method with dopamine and polyethyleneimine, Sep. Purif. Technol. 212 (2019) 641–649.
[75] Y. Zhang, Y. Jia, M. Li, L.a. Hou, Influence of the 2-methylimidazole/zinc nitrate hexahydrate molar ratio on the synthesis of zeolitic imidazolate framework-8 crystals at room temperature, Scientific reports, 8 (2018) 1-7.
[76] T. Zhang, X. Zhang, X. Yan, L. Kong, G. Zhang, H. Liu, J. Qiu, K.L. Yeung, Synthesis of Fe3O4@ ZIF-8 magnetic core–shell microspheres and their potential application in a capillary microreactor, Chem. Eng. J. 228 (2013) 398–404.
[77] A. Schejn, L. Balan, V. Falk, L. Aranda, G. Medjahdi, R. Schneider, Controlling ZIF-8 nano-and microcrystal formation and reactivity through zinc salt variations, CrystEngComm 16 (2014) 4493–4500.
[78] A. Gong, C.-T. Zhu, Y. Xu, F.-Q. Wang, F.-A. Wu, J. Wang, Moving and unsinkable graphene sheets immobilized enzyme for microfluidic biocatalysis, Sci. Rep. 7 (2017) 1–15.
[79] B. Tomaszewski, A. Schmid, K. Buehler, Biocatalytic production of catechols using a high pressure tube-in-tube segmented flow microreactor, Organic Process Res. Develop. 18 (2014) 1516–1526.
[80] Y. Zhao, C. Yao, G. Chen, Q. Yuan, Highly efficient synthesis of cyclic carbonate with CO 2 catalyzed by ionic liquid in a microreactor, Green Chem. 15 (2013) 446–452.
[81] A. Alam, K.-Y. Kim, Analysis of mixing in a curved microchannel with rectangular grooves, Chem. Eng. J. 181 (2012) 708–716.

[82] A.D. Stroock, S.K. Dertinger, G.M. Whitesides, A. Ajdari, Patterning flows using grooved surfaces, Anal. Chem. 74 (2002) 5306–5312.
[83] V. Asadi, R. Kardanpour, S. Tangestaninejad, M. Moghadam, V. Mirkhani, I. Mohammadpoor-Baltork, Novel bovine carbonic anhydrase encapsulated in a metal–organic framework: a new platform for biomimetic sequestration of CO 2, RSC Adv. 9 (2019) 28460–28469.
[84] K. Jähnisch, M. Baerns, V. Hessel, W. Ehrfeld, V. Haverkamp, H. Löwe, C. Wille, A. Guber, Direct fluorination of toluene using elemental fluorine in gas/liquid microreactors, J. Fluorine Chem. 105 (2000) 117–128.
[85] J. Kobayashi, Y. Mori, S. Kobayashi, Hydrogenation reactions using scCO 2 as a solvent in microchannel reactors, Chem. Commun. (2005) 2567–2568.
[86] N. De Mas, A. Günther, M.A. Schmidt, K.F. Jensen, Microfabricated multiphase reactors for the selective direct fluorination of aromatics, Industr. Eng. Chem. Res. 42 (2003) 698–710.
[87] X. Liu, X. Yu, Enhancement of butanol production: from biocatalysis to bioelectrocatalysis, ACS Energy Lett. 5 (2020) 867–878.
[88] X. Liu, L. Shi, J.-D. Gu, Microbial electrocatalysis: redox mediators responsible for extracellular electron transfer, Biotechnol. Adv. 36 (2018) 1815–1827.
[89] Y. Chen, P. Li, H. Noh, C.W. Kung, C.T. Buru, X. Wang, X. Zhang, O.K. Farha, Stabilization of Formate Dehydrogenase in a Metal-Organic Framework for Bioelectrocatalytic Reduction of CO2, Angew. Chem. 131 (2019) 7764–7768.
[90] R. Barin, D. Biria, S. Rashid-Nadimi, M.A. Asadollahi, Enzymatic CO2 reduction to formate by formate dehydrogenase from Candida boidinii coupling with direct electrochemical regeneration of NADH, J. CO2 Util. 28 (2018) 117–125.
[91] S.K. Kuk, K. Gopinath, R.K. Singh, T.-D. Kim, Y. Lee, W.S. Choi, J.-K. Lee, C.B. Park, NADH-free electroenzymatic reduction of CO2 by conductive hydrogel-conjugated formate dehydrogenase, ACS Catal. 9 (2019) 5584–5589.
[92] S.K. Yoon, E.R. Choban, C. Kane, T. Tzedakis, P.J. Kenis, Laminar flow-based electrochemical microreactor for efficient regeneration of nicotinamide cofactors for biocatalysis, J. Am. Chem. Soc. 127 (2005) 10466–10467.
[93] S. Fornera, P. Kuhn, D. Lombardi, A.D. Schlüter, P.S. Dittrich, P. Walde, Sequential immobilization of enzymes in microfluidic channels for cascade reactions, ChemPlusChem 77 (2012) 98–101.
[94] P. Trens, R. Durand, B. Coq, C. Coutanceau, S. Rousseau, C. Lamy, Poisoning of Pt/C catalysts by CO and its consequences over the kinetics of hydrogen chemisorption, Appl. Catal. B 92 (2009) 280–284.
[95] X. Ji, K.T. Lee, R. Holden, L. Zhang, J. Zhang, G.A. Botton, M. Couillard, L.F. Nazar, Nanocrystalline intermetallics on mesoporous carbon for direct formic acid fuel cell anodes, Nat. Chem. 2 (2010) 286–293.
[96] N. Kristian, Y. Yan, X. Wang, Highly efficient submonolayer Pt-decorated Au nanocatalysts for formic acid oxidation, Chem. Commun. (2008) 353–355.
[97] J. Xu, T. Zhao, Z. Liang, Synthesis of active platinum− silver alloy electrocatalyst toward the formic acid oxidation reaction, J. Phys. Chem. C 112 (2008) 17362–17367.